Deficiency of *ZC3HC1* increases vascular smooth muscle cell migration, proliferation and neointima formation following injury

Redouane Aherrahrou (1,2)*, Tobias Reinberger (1)*, Julia Werner (4), Miriam Otto (1), Jaafar Al-Hasani (1), Maria Loreto Munoz-Venegas (1), Mete Civelek (2,3), Heribert Schunkert (4), Thorsten Kessler (4), Jeanette Erdmann (1)#, Zouhair Aherrahrou (1)#

(1) Institute for Cardiogenetics, Universität zu Lübeck; DZHK (German Centre for Cardiovascular Research), Partner Site Hamburg/Kiel/Lübeck, Germany; University Heart Centre Lübeck, 23562 Lübeck, Germany

(2) Center for Public Health Genomics, University of Virginia, Charlottesville, VA, USA

(3) Department of Biomedical Engineering, University of Virginia, Charlottesville, VA, USA

(4) Deutsches Herzzentrum München, Technische Universität München and DZHK (German Centre for Cardiovascular Research); Partner Site Munich Heart Alliance, München, Germany

Running title: *Zc3hc1* protects against neointima formation

* / #: These authors contributed equally to this work

Corresponding author: Dr. Zouhair Aherrahrou

Institute for Cardiogenetics, Universität zu Lübeck, Ratzeburger Allee 160, 23562 Lübeck, Germany

Tel: +49 451 3101 8310; Fax: +49 451 3101 8308; E-mail: zouhair.aherrahrou@uni-luebeck.de

Abstract:

The *ZC3HC1* gene is associated with various cardiovascular traits in that its common missense variant, rs11556924-T (p.Arg363His), lowers risk of coronary artery disease (CAD) and blood pressure, but increases carotid intima-media thickness (IMT). This study was designed to determine the mechanisms by which *ZC3HC1* modulates IMT using *in vitro* and *in vivo* models.

We assessed the effect of the rs11556924-T allele on *ZC3HC1* expression in vascular smooth muscle cells (SMCs) from 151 multi-ethnic heart transplant donors and found that rs11556924-T was significantly associated with lower *ZC3HC1* expression and faster SMC migration. These results were supported by *in vitro* silencing experiments. At the protein level, *ZC3HC1* deficiency resulted in the accumulation of cyclin B1, a key cell cycle protein. Further, transcriptome analysis revealed changes in the regulation of canonical SMC marker genes, including *ACTA2*, *CNN1*, *LMOD1*, and *TAGLN*. Pathway analysis of differentially expressed genes in SMCs secondary to *ZC3HC1* knockdown showed decreased expression of genes in the cell division and cytoskeleton organization pathways.

In line, primary SMCs isolated from the aortas of *Zc3hc1*$^{-/-}$ mice migrated faster and proliferated more compared to SMCs isolated from wild-type littermates, with the former also showing accumulation of cyclin B1. Neointima formation was also enhanced in *Zc3hc1*$^{-/-}$ mice in response to arterial injury mimicking restenosis.

Taken together, these findings demonstrate that genetic modulation or deficiency of *ZC3HC1* leads to the accumulation of cyclin B1 in SMCs and increased migration, proliferation, and injury-induced neointima formation. We further discuss and propose that a genetic variant regulating SMC proliferation may enhance IMT and early atherosclerosis progression but may be beneficial for plaque stability in advanced lesions.

Key words: *ZC3HC1*, NIPA, SMC migration and proliferation, neointima formation, *cyclin B1*.

Introduction: Coronary artery disease (CAD) caused by atherosclerosis is the leading cause of death in the developed world [1]. Due to atherosclerotic deposits, the lumen of the vessels becomes narrow, limiting the supply of oxygen-rich blood to the affected tissue. This reduction in blood flow may result clinically in the development of chest pain and, in the event of atherothrombosis or myocardial infarction (MI). Implantation of coronary stents is the primary therapeutic option to reopen an occluded coronary artery in MI patients. Despite the development of drug-eluting stents and balloons, restenosis due to neointima formation remains a major limitation after coronary intervention.

Genome-wide association studies (GWAS) have identified the single nucleotide polymorphism (SNP) rs11556924 at chromosome 7q32.2 CAD susceptibility locus, which harbors the *ZC3HC1* gene [2–8]. The CAD-associated variant rs11556924-T is a non-synonymous variant, leading to an amino acid substitution p.Arg363His in the canonical transcript of *ZC3HC1* and a ~4.9% to 7.0% reduction in CAD risk per allele [4,6,9,10]. However, the same genetic variant increases the risk of carotid intima-media thickness (IMT) in patients with rheumatoid arthritis [11].

ZC3HC1 encodes the nuclear-derived protein, nuclear interaction partner of anaplastic lymphoma kinase (NIPA)[12], an essential component of the SCF-type E3 ubiquitin ligase complex that initiates the degradation of cyclin B1 [7,13]. Because cyclin B1 and cyclin-dependent kinase form the M-phase promoting factor, NIPA is involved in regulating the cell cycle at the G2 to M-phase transition [13].

To understand the link between NIPA modulation and vascular remodeling, we assessed the role of *ZC3HC1* in human and murine vascular smooth muscle cells (SMCs), a key cell type involved in neointima formation following injury [14]. Specifically, we analyzed the effects of *ZC3HC1* on migration and proliferation of primary human and mouse aortic SMCs *in vitro*. Subsequently, we used wire injury to induce neointimal hyperplasia [15] *in vivo* in *Zc3hc1*-deficient mice. Our findings showed that *ZC3HC1* deficiency was accompanied by cyclin B1 accumulation, increased migration and proliferation of vascular SMCs and enhanced neointima formation.

Material and Methods

Expression quantitative trait locus analysis of ZC3HC1 in human SMCs: The University of Virginia IRB has ruled that specimens used for cell collection do not fall under the purview of current regulations governing the participation of human subjects in research since these specimens have no identifying information. This study was approved by the Institutional Review Boards of UCLA and the University of Virginia.

Human aortic SMCs isolated from the ascending aortas of 151 heart transplant donors at UCLA or obtained from commercial suppliers (Lonza and PromoCell) as this has been previously described [16]. All SMCs were maintained in Smooth muscle cell Basal Medium (SmBM, CC-3181, Lonza) supplemented with Smooth muscle Medium-2 (SmGM-2, CC-4149, Lonza). Briefly, the stranded libraries of high-quality ribosomal RNA-depleted total RNA were sequenced to ~100 million read depth with 150 bp paired-end reads at the Psomogen sequencing facility. The reads with average Phred scores <20 were trimmed using Trim Galore, followed by mapping the reads to the hg38 version of the human reference genome using the STAR Aligner[17] in two-pass mode. Gene expression of *ZC3HC1* was quantified by calculating the number of transcripts per million (TPM) using RNA-SeQC[18]. Expression quantitative traits locus (eQTL) analysis was performed using tensorQTL[19] after correcting for sex, genotype PCs, and hidden confounding variables.

Quantification of migration in 151 primary SMCs: Cell migration assays were performed with the xCELLigence Biosensor System using specifically designed 16-well plates equipped with membranes having 8-μm pores (CIM-plate 16; Roche Diagnostics). Cells in serum-free medium were seeded in the upper chambers, and the chemoattractant PDGF-BB (100 ng/mL) added to the lower chambers, with serum-free medium being the negative control. Cell migration was monitored over 24 h. Data were analyzed using RTCA software version 1.2 (Acea Biosciences Inc., San Diego, CA) combined with R software. The association between the genotype of rs11556924 and migration was calculated using linear mixed model to account for multiethnic population composition as previously been described [16].

Silencing of ZC3HC1 gene expression using siRNA: Dicer small interfering RNA (siRNA) targeting the *ZC3HC1* gene (*ZC3HC1* siRNA, IDT-ID: hs.Ri.ZC3HC1.13.2) and scramble control siRNA were purchased from Integrated DNA Technologies (IDT). Human aortic SMCs (Cell Applications, Inc., #354-05a, C/C genotype for rs11556924) in M231 cell culture

medium (Gibco) with Smooth Muscle Growth Supplement (SMGS) (Gibco) were cultured in 48-well cell culture plates (Greiner bio-one) at a density of 0.4×10^5 cells per well for 24 h. The cells were transfected with 5 nM *ZC3HC1* siRNA or 5 nM control siRNA overnight using GenMute™ SMC siRNA Transfection Reagent (SignaGen Laboratories) according to the manufacturer's instructions. The transfected cells were subsequently incubated in M231 SMGS culture medium for 48 h, after which the samples were harvested and stored at -80°C until used for qPCR and Western blot analyses.

Cell migration and proliferation of ZC3HC1-KD SMCs: To determine the role of *ZC3HC1* gene expression knockdown in SMC migration, wound-healing assays with ibidi 4-well culture inserts in a 12-well plate format were performed as described[20]. Briefly, approximately 2.2×10^4 SMCs (Cell Applications, Inc., #354-05a, C/C genotype for rs11556924) per well were seeded into insert wells and incubated at 37°C and 5% CO_2 for 24 h. Following siRNA transfection overnight (see above), the cells were incubated in M231 culture medium supplemented with Smooth Muscle Differentiation Supplement (SMDS) (Gibco), which contains only 1% (v/v) fetal bovine serum (FBS) and 30 µg/mL heparin. After 48 h, the inserts were removed, and the cells were washed with phosphate buffered saline (PBS) and cultured in M231 SMDS medium supplemented with 5 ng/mL PDGF-BB (Peprotech) to provoke cell migration. Images taken at 0 and 12 h with an Olympus IX70 microscope were analyzed using an in-house Python script. In brief, images were converted into black-and-white images and optimized using the methods *GaussianBlur* and *adaptiveThreshold* in the OpenCV package *cv2*. The mean pixel distances were calculated relative to time 0. All experiments were performed in triplicate. To assess the proliferation of *ZC3HC1*-KD SMCs, the cells were plated into 96-well plates (0.6×10^4 cells/well) and transfected as described above. The next day, the cell culture medium was replaced by M231 medium supplemented with 1% FBS to starve the cells. These human SMCs were subsequently treated with 100 ng/mL PDGF-BB (Peprotech) to induce proliferation. To quantify the proliferation rate, the cell nuclei were stained with Hoechst 33342 dye (ThermoFisher Scientific) at several time points and the number counted using an in-house Python script *CellCounter.py*. Six wells were analyzed per condition, with all experiments performed in triplicate. The values were normalized to time point zero to account for small differences in initial cell numbers after siRNA transfection.

qPCR analysis: These analyses were performed as described [21] [22]. Briefly, total RNA was isolated from cultured cells using RNeasy plus kits (Qiagen, Valencia, CA, USA) and reverse transcribed into cDNA. mRNA levels were determined by relative quantitative RT-PCR and analyzed using the ΔΔCT method relative to the internal standard, GAPDH [21]. The primers (Eurofins Genomics) used in this study are shown in **Table 1**.

Table 1: Primer sequences used in qPCR reactions.

Gene	Forward primer (5' - 3')	Reverse primer (5' - 3')	Expected fragment length (bp)
ACTA2	*TAGAACATGGCATCATCACCA*	*AGGGTGGGATGCTCTTCAG*	100
CALD1	*GAGTCCTCCAGTGTCTTGGC*	*GCCCTGGTTAGCTCTTCTGG*	184
CCNB1	*GCCAGAACCTGAGCCTGTTA*	*CAGAGAAAGCCTGACACAGGT*	131
CNN1	*GTTGGCCTCAAAAATGTCGT*	*AGGCTCCGTGAAGAAGATCA*	121
GAPDH	*AGATTTGGTCGTATTGGG*	*GGAAGATGGTGATGGGATT*	203
LMOD1	*GCTCAACTTCTGTGAAAAGGAGA*	*TCTTGGCATCTGTCTTGGTCT*	95
TAGLN	*CACCAGCTTGCTCAGAATCA*	*GTCCTTCCTATGGCATGAGC*	185
TPM1	*TGAGAAGGCAGCAGATGAGA*	*GTCGGCATCTTCAGCAATG*	130
ZC3HC1	*CTGGCCAGACAGCCCATC*	*GAAGCTGGAGGTCCAAGTGA*	119

Western blot analysis: Western blot analyses were performed as described [22]. Briefly, 15 µg samples of protein isolated from cultured cells were electrophoresed on SDS-PAGE gels and transblotted onto nitrocellulose membranes. The blots were treated with 5% skim milk and incubated with primary antibodies, including anti-NIPA (phospho S354) antibody (abcam ab63557), anti-cyclin B1 antibody (abcam ab181593) and anti-GAPDH antibody (loading control; abcam ab181602). The blots were subsequently incubated with the appropriate secondary antibodies. Protein bands were detected using the ECL Prime Western Blotting Detection Reagent (GE Health Care) and quantified using ImageLab software (Bio-Rad).

RNA sequencing: Human aortic SMCs (Cell Applications, Inc., #354-05a) were seeded into 6-well plates at a density of 3.1×10^4 cells/cm^2 and transfected with siRNA as described above. After 2 days in M231 SMDS medium, 5 ng/mL PDGF-BB (Peprotech) were added. Cells devoid of PDGF-BB served as an internal control. After incubation for 24 h, the RNA was extracted using innuPREP RNA Mini Kits 2.0 (Analytik Jena), yielding ~5 µg total RNA (RIN>7) per sample. RNA sequencing (RNAseq), including ribosomal RNA-depletion and quality control, was performed at the Novogene sequencing facility (NovaSeq 6000 PE150,

150 bp paired-end reads). After trimming reads with low average Phred scores (<20) using Trim Galore, all included samples passed the quality control analysis. Reads were mapped to the hg38 version of the human reference genome using the STAR Aligner[17] in two-pass mode, with gene expression quantified by calculating TPM using RNA-SeQC[18].

Differential gene expression and functional enrichment analysis: A total of 17,242 genes with >6 reads were included in at least 20% of the samples in at least one of the two conditions (ZC3CH1 siRNA and control siRNA) for differential expression analysis using DESeq2 controlling for batch effect [23]. Genes were considered to be differentially expressed under treated and untreated conditions when p_{adj} was <0.05 and $\log_2$(fold-change) was >0.5. Principal component analysis (PCA) was performed using R. PDGF-BB treatment was defined as a covariate. Network analysis and Gene Ontology (GO) enrichment after clustering were performed to characterize the functional consequences of differences in gene expression associated with downregulation and normal expression of *ZC3HC1* [24]. In brief, a functional gene network containing differentially expressed genes (p_{adj}<0.05) was constructed with the help of the STRING database repository (https://string-db.org/) using the REST API implemented in Python. The following parameters were used: species: 9606, network_type: functional, network_flavor: confidence, score>0.4, add_white_nodes: 30 for the complete gene network (**Supplementary Figure 2**) and 8 for the CCNB1 subnetwork (**Figure 3**). Agglomerative ward clustering of the gene network was performed using the *scikit-learn* (version 0.24.2) clustering package. Gene set enrichment of each cluster was performed using the REST API of STRING[24]. Gene networks were visualized by the Python packages *networkx* (V4.4.0) and *matplotlib* (V40.8.0).

Generation and housing of animals: Heterozygous *Zc3hc1* ($^{+/-}$) mice (Zc3hc1tm1a(KOMP)Wtsi, background: C57BL/6N) were obtained from KOMP at UC Davis, California. They were created using a targeting construct of the mouse *Zc3hc1* gene, designed by introducing the EN2 splicing acceptor (EN2 SA) followed by the beta-galactosidase sequence and a neomycin selection cassette 3' at exon 4. Heterozygous mice were initially backcrossed to a C57BL/6J genetic background for at least six generations and then used in Het × Het mating to generate sufficient numbers of *Zc3hc1* knockout (KO or $^{-/-}$) and wild-type (WT or $^{+/+}$) littermates for the experiments. Homozygous *Zc3hc1* ($^{-/-}$) were found to be infertile. Mice were genotyped using PCR screenings of DNA samples isolated from ear biopsies. Mice were genotyped using the primers 5'-TTGACTGACAGAGGATGAGAGC-3' (forward) and 5'-GGGCCTTTAATCCCAACACT-

3' (reverse), targeting the second *LoxP* site located between exons five and six in the *Zc3hc1* gene. The expected lengths of the DNA fragments were 298 bp for the knockout and 260 bp for the WT mice (**Figure 4A, right**). In addition, β-gal-activity was measured in heart cryosections from one mouse per genotype (*Zc3hc1* $^{+/+}$, or $^{-/-}$) (**Supplementary Figure 3C**), as described [25].

Neointima formation mouse model: All animal experiments were performed in accordance with the German animal studies committee of Upper Bavaria and under international guidelines. Wire injury was induced in 8- to 12-week-old female mice as described [18]. Briefly, all surgical procedures were performed under general anesthesia. Anesthesia was achieved by intraperitoneal (i.p.) injection of midazolam (5.0 mg/kg), medetomidine (0.5 mg/kg), and fentanyl (0.05 mg/kg) (MMF) in 300µl of 0.9% (w/v) sodium chloride. A half dosage of MMF was added if the inter-toe reflex was re-established or the duration of anesthesia exceeded 60 minutes. After a skin incision, the left femoral artery of each was exposed by blunt dissection and an angioplasty guidewire (0.015 inch in diameter, No. C-SF-15-15, COOK, Bloomington, IN) was introduced into the arterial lumen and inserted towards the iliac artery. To denude and dilate the femoral artery, the wire was left in place for 1 minute. The guidewire was then removed and the arteriotomy site ligated. Mice were sacrificed 14 days later by i.p. injection of pentobarbital. To remove blood inside the femoral arteries, the mice were perfused via the left ventricle and over the descending aorta with PBS (pH= 7.4). Femoral arteries were harvested and fixed in 4% buffered paraformaldehyde overnight.

***Histology and morphology*:** Paraffin-embedded femoral arteries were sectioned at 2-µm intervals and stained with hematoxylin and eosin. For morphometric analysis, images were digitalized (Leica DFC450C camera) and serial sections in 50-µm intervals of each artery were blindly analyzed using ImageJ software (NIH Image Software). Media thickness (M) and the area of neointima formation (NI) were quantified and neointima-to-media ratios (NI/M) were calculated. To count Ki-67 positive cells, sections of paraffin-embedded femoral arteries were de-paraffined through a series of decreasing concentrations of alcohol (3x xylol, 2× 100% ethanol, 1× 96% ethanol, 1× 70% ethanol and deionized water). The slides were heated for 1.5 min in a microwave at 900 W and for 15 min at 90 W. For histochemistry**,** the slides were washed three time with PBS and unspecific binding was blocked by incubation with 5% (v/v) goat serum in PBS. Tissue slides were stained overnight at ambient temperature with anti-Ki-67 (1:100 in PBS, ThermoFisher Scientific, Clone:B56, #15898578) or anti-

ACTA2 (1:100 in PBS, Abcam ab5694) antibody, and primary antibodies were visualized using a horseradish peroxidase system (Santa Cruz, SC2004) and DAB staining solution (DAKO, #3468). Cell nuclei were stained using a hemotoxylin solution (Carl Roth, #T865.1). To fix the slides, they were treated with a series of increasing concentrations of alcohol (see above), followed by treatment with Cytoseal XYL (ThermoFisher Scientific #8312-4).

Isolation and culture of murine SMCs: Mouse aortic SMCs were isolated from the thoracic aortas of WT and KO (*n*=8-10) as reported previously [22]. Briefly, the thoracic aortas were collected, and fat and connective tissues were removed. The samples were pre-digested with collagenase II and the adventitia was removed mechanically. Adventitia-free aortas were cut into small pieces and further digested with collagenase II with shaking for at least 6 h, until complete tissue dissociation. The isolated cells were pelleted and resuspended in culture medium (DMEM plus 10% FBS and 1% penicillin/streptomycin, Gibco). Cells were expanded and grown on surfaces coated with 0.1% (w/v) gelatin. To quantify the purity of the populations, the isolated cells were characterized by flow cytometry using the SMC-specific FITC-labeled anti-α-SMA antibody (Sigma, F3777) and an isotype control (mouse IgG2a-FITC, Sigma F6522), yielding >95% purity (**Supplementary Figure 4**).

Murine SMC migration and proliferation: The migration of murine aortic SMCs was assessed using the xCELLigence RTCA DP system as described above. Briefly, the electrode side of the membrane was coated with 0.1% gelatin. The bottom compartment of each well was filled with 165 µL of culture medium or serum-free medium as a control, and the membrane compartment was mounted. The upper wells were filled with 50 µL of serum-free medium and equilibrated for 1 h at 37 °C in an incubator. Cell concentrations were adjusted to 2.7×10^4 cells/mL per well. Data were recorded for 24 h. To quantify the proliferation of murine aortic SMCs, cells were seeded in 12-well plates to yield a confluency of ~30%. To make these results comparable to those of the proliferation assay for human SMCs transfected with siRNA, the cells were incubated for 1 day, with the timepoint 0 h defined as 24 h after seeding. At each given timepoint, the cells were washed once with 1 mL PBS and fixed with 0.5 mL of 4% (v/v) paraformaldehyde (PFA) for 5 min. After removing the PFA, the cells were permeabilized with 0.5 mL Triton-X-100 for 10 min, washed with 1 mL PBS, and stained with 0.5 mL 4',6-diamidino-2-phenylindole, dihydrochloride (DAPI) solution for 10 min in the dark. After acquiring images of 10 non-overlapping regions per well, both the cell number and average size of nuclei were determined using our in-house Python script

CellCounter.py. Proliferation assays were performed in triplicate. The results were normalized to time point zero for each condition and replicate.

Statistical Analysis: All data are presented as the mean ± standard deviation (SD), with two groups compared by unpaired Student's t-tests or Mann–Whitney U tests ($n<8$ or not normally distributed data). All statistical analyses were performed using R or Python libraries, with $p<0.05$ considered statistically significant.

Results

Associations of the *ZC3HC1* variant rs11556924-T with cardiovascular disease (CVD)-related phenotypes: A hypothesis-free phenome scan was performed using the MR-Base PheWAS online tool[26] and the GWAS Catalog[27] to determine the associations of rs11556924 variants with CVD-related phenotypes. As expected, a genome-wide significant association was observed between this SNP and cardiovascular-related traits, including hypertension and CAD (**Figure 1A**, **Supplementary Table 1**), with the rs11556924-T allele associated with reduced risk of these diseases. A suggestive association ($p=1.4 \times 10^{-5}$) was also observed between this SNP and mean carotid IMT in the MRC-IEU consortium data (**Supplementary Table 1**).

The rs11556924-T SNP is associated with lower *ZC3HC1* expression and higher migration in human SMCs: To understand the role of the rs11556924 variant at the level of gene expression, an eQTL analysis was performed using SMCs of 151 human donors. This assay showed that the T allele was associated ($p=0.012$) with lower *ZC3HC1* expression (**Figure 1B**). To our knowledge, there are no eQTLs in monocytes/macrophages[28] or aortic endothelial cells[29], suggesting that the regulatory impact of rs11556924 in the *ZC3HC1* locus is SMC specific. Therefore, we assessed the impact of this variant on SMC migration, a hallmark for vascular remodeling [14]. Cell migration assays were performed using 100 ng/mL PDGF-BB as a chemoattractant in serum-free media, as described previously [16]. SMCs carrying the rs11556924-T variant were found to migrate faster toward PDGF-BB than SMCs carrying the C allele (**Figure 1C**), also after adjusting for sex. This result suggests that the *ZC3HC1* rs11556924 variant is independent of the traditional CAD risk factors, such as male sex [30,31].

Downregulation of *ZC3HC1* in human SMC increases migration and proliferation: To further investigate how *ZC3HC1* modulation affects SMC migration, cells were transfected with siRNA against *ZC3HC1* (*ZC3HC1* siRNA; knockdown efficiency was ~70% 12 h after transfection (**Figure 1D**)) or control siRNA. Migration assays showed that transient siRNA mediated knockdown of *ZC3HC1* transcripts promoted cell migration (**Figure 1E-F**). Moreover, adding PDGF-BB was accompanied by lower expression of *ZC3HC1* in control SMCs (**Figure 1D**) and increased migration (**Figure 1E**) in both *ZC3HC1*-KD and control SMCs ($p<0.001$). However, a significant difference between *ZC3HC1*-KD and control SMCs was apparent in both the presence and absence of PDGF-BB. In addition, a lower level of *ZC3HC1* mRNA significantly enhanced the proliferation of SMCs at 72 h, but not at earlier time points. This finding was in agreement with the results from genotyped SMCs derived from 151 human donors[16], in which no significant correlation was observed between the T allele and cell proliferation at 24 h.

Transcriptional profiling of *ZC3HC1* downregulation in human SMCs: To determine the transcriptional profile of *ZC3HC1* downregulation, transcriptome analysis using RNA sequencing was performed in aortic SMCs in the presence or absence of 5 ng/mL PDGF-BB. After quality control and quantification, the number of expressed genes (defined as genes with more than six read counts in at least 20% of the samples) ranged from 16,880 under control conditions to 17,242 after treatment with PDGF-BB (**Supplementary Table 5**). PCA identified two distinct clusters of samples, corresponding to the cells cultured under the two conditions with endogenous *ZC3HC1* expression and *ZC3HC1* downregulation (**Supplementary Figure 1**). Further, 3,045 genes were differentially expressed ($p_{adj}<0.05$). Of these, 284 genes showed a $\log_2$(fold-change [FC]) above 0.5 (median 0.68), and 179 genes were downregulated with $\log_2(FC)<-0.5$ (median -0.67). The latter also include the canonical SMC markers *LMOD1*, *TPM1*, *CNN1*, *CALD1*, *ACTA2*, and *TAGLN* (**Figure 2A-B**). Downregulation of the expression of genes encoding SMC markers in response to *ZC3HC1* knockdown was confirmed by qPCR (**Figure 2C**).

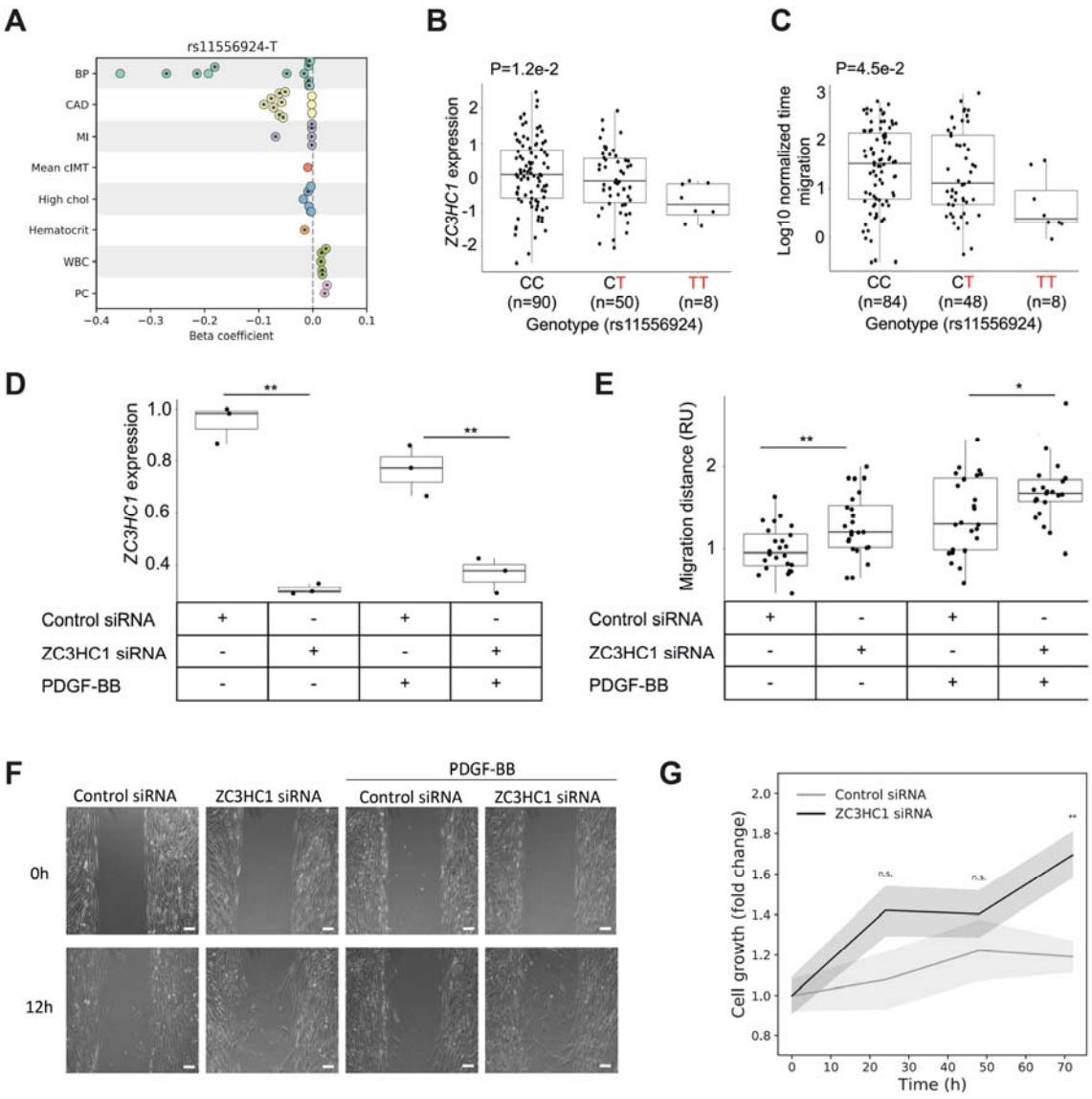

Figure 1. Association of rs11556924 with cardiovascular diseases predominantly driven by vascular SMC dysfunction, *ZC3HC1* expression and vascular SMC migration. A) Predominant association of rs11556924 with cardiovascular disease (CVD) driven by vascular SMC dysfunction. The plot shows the beta effect size of the rs11556924-T allele derived from several genome-wide association studies (GWAS) categorized according to eight CVD-related traits (BP, blood pressure; CAD, coronary artery disease; MI, myocardial infarction; cIMT, carotid intima-media thickness; chol, cholesterol; WBC, white blood cell count; PC, platelet count). Asterisks indicate genome-wide significance ($p<5 \times 10^{-8}$); data points without asterisks represent genome-wide associations with suggestive significance ($p<5 \times 10^{-5}$). Negative effect size indicates that the risk allele (T) of the single nucleotide polymorphism, rs11556924, is associated with a lower risk for several traits, including blood pressure or coronary artery disease. **B)** The risk allele (T) of rs11556924 is associated with lower *ZC3HC1* expression and **C)** faster migration by vascular SMCs. SMCs transfected with siRNA against *ZC3HC1* showed significant **D)** *ZC3HC1* downregulation and **E)** increased migration in the presence or absence of PDGF-BB (n=3, eight images per replicate). **F)** Representative images of the migration of SMCs transfected with *ZC3HC1* siRNA and control siRNA (scale bars, 100 µm). **G)** Knockdown of *ZC3HC1* resulted in significant increases in cell proliferation in the presence of PDGF-BB. Values are shown as means. The translucent error bands represent s.d. * $p<0.05$; ** $p<0.01$; n.s., not significant. Data in **B**, **C**, and **E** were analyzed using unpaired Student's t test. Others were analyzed using Mann-Whitney U test.

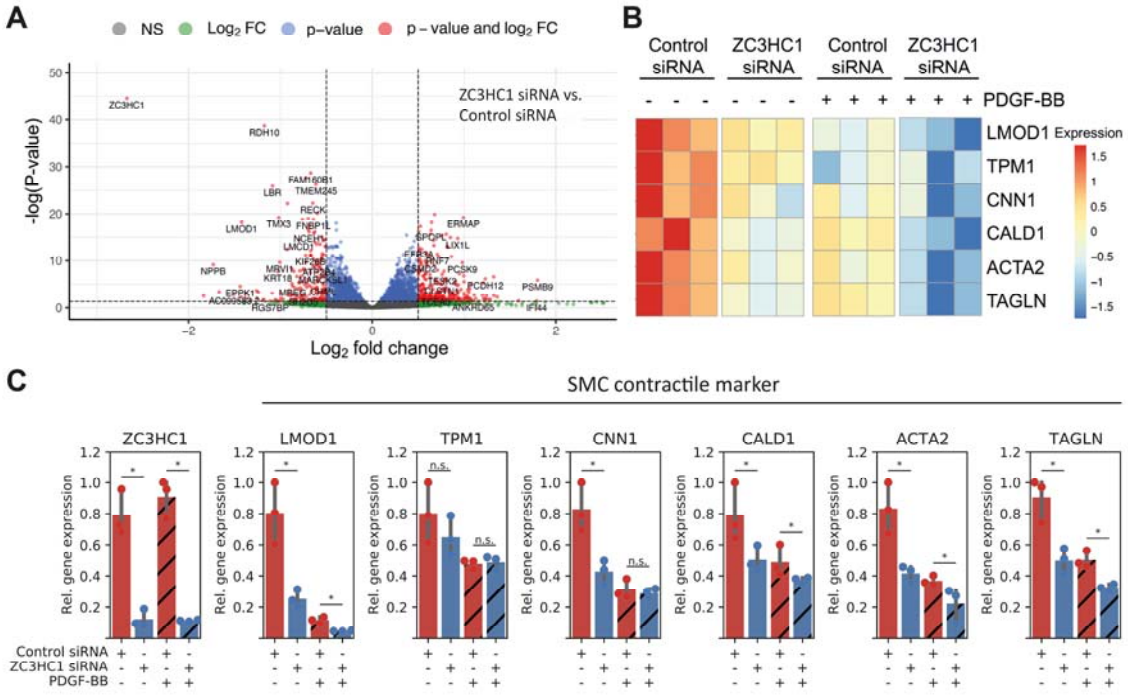

Figure 2. Transcription profiling of human SMC after *ZC3HC1* downregulation. A) Volcano plot of the expression profiles of differentially expressed genes in SMCs transfected with siRNA against *ZC3HC1* (*ZC3HC1* siRNA) (n=4) and control siRNA (n=5). The red data points represent the differentially expressed genes with statistical significance, whereas the gray data points indicate genes without disturbed gene expression. The vertical dashed lines correspond to a 0.5-fold-change in gene expression (up or down), and the horizontal dashed line represents the adjusted p-value for each gene. **B)** Heat map showing contractile SMC marker genes that were differentially expressed upon knockdown of *ZC3HC1* (from the same batch) in the presence or absence of PDGF-BB. **C)** qPCR validation of the expression of the contractile SMC marker genes. Values are shown as mean ± s.d.; * $p<0.05$; n.s., not significant. Data in **C** were analyzed using Mann-Whitney U test.

Network analysis of differentially expressed genes

Subsequent network analysis of differentially expressed genes ($p_{adj}<0.05$ and $abs(\log_2(FC))>0.4$) using the STRING database[24] revealed that the *CCNB1* gene encoding cyclin B1 is a central hub for a variety of gene clusters (**Figure 3A-B, Supplementary Figure 2 and Supplementary Table 6-8**), whereas *ZC3HC1* interacted only with *CCNB1* (STRING score=0.607). Therefore, network analysis indicated that modulation of *ZC3HC1*/NIPA predominantly induces transcriptional changes through cyclin B1. Additional enrichment analysis of gene clusters highlighted several biological processes that were apparently modulated by the knockdown of *ZC3HC1*, including protein ubiquitination, muscle contraction/ cytoskeleton organization, and cell division (**Figure 3B**). To test whether *CCNB1* is modulated by lower levels of *ZC3HC1* in SMCs, we performed co-expression and Western blot analyses. Analysis of gene expression in aortic SMCs of 151 individuals showed a positive correlation ($R=0.59$; $p=1.4 \times 10^{-15}$) between *ZC3HC1* and *CCNB1* at the RNA level (**Figure 3C**, top panel). Similarly, qPCR showed that siRNA mediated *ZC3HC1*

downregulation reduced *CCNB1* expression in SMCs (**Figure 3C**, top right). At the protein level, however, a lack of NIPA resulted in the intracellular accumulation of cyclin B1 (**Figure 3C** bottom panel), as previously described [13].

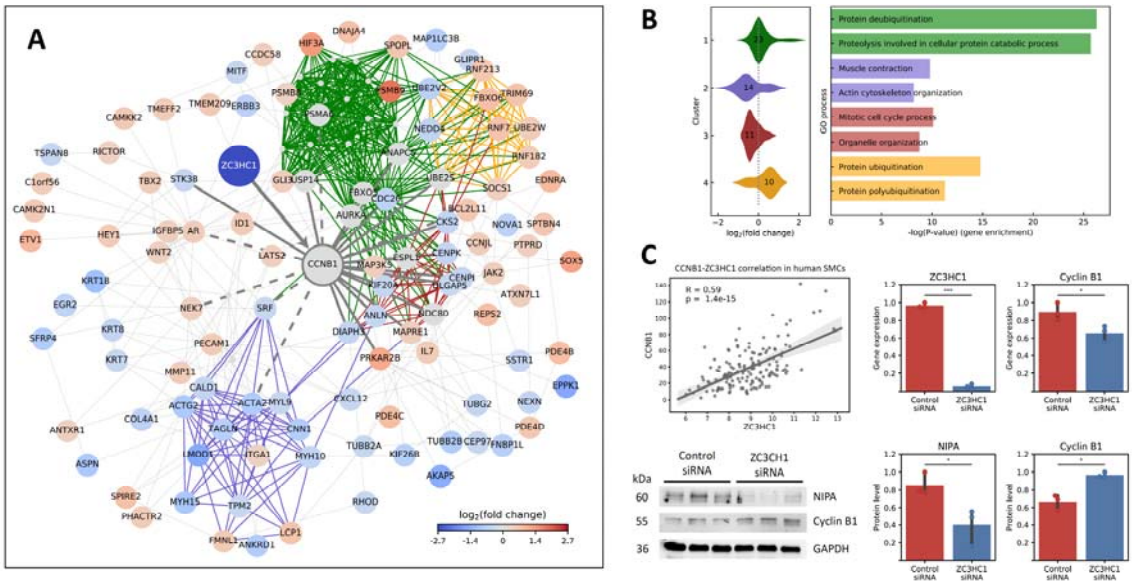

Figure 3. Gene interaction network of *ZC3HC1*/CCNB1 in SMCs and accumulation of cyclin B1 by *ZC3HC1* knockdown. A) Effect of *ZC3HC1* knockdown on the cyclin B1 (CCNB1) subnetwork of differentially expressed genes (adjusted p-value <0.05 and abs(log_2(fold-change))>0.4) derived from the STRING database. The edges represent the combined STRING scores (>0.4, median=0.9) derived from co-expression, experimental, database, and text mining scores. The complete gene interaction network is shown in **Supplementary Figure 2**. The fold changes in gene expression on the log_2-scale are depicted by red and blue spheres. Gray spheres indicate genes not differing in expression but interacting with CCNB1 or neighboring genes according to the STRING database. Gray bold lines indicate direct interactions with CCNB1 with medium to high confidence (scores >0.5), and dashed lines indicate direct interactions with lower confidence (score=0.4–0.5). Colored lines represent gene clusters. **B)** Distribution of log_2(fold changes) in gene expression for each cluster and enriched biological processes derived from Gene Ontology. Numbers in the violin plot indicate the number of genes in the cluster. **C)** Co-expression analysis in 151 human aortic SMC preparations showed a positive correlation between *ZC3HC1* and *CCNB1* gene expression, which was confirmed by transient knockdown of *ZC3HC1* and qPCR (right top corner). By contrast, Western blot showing that *ZC3HC1* knockdown results in the accumulation of cyclin B1 protein in SMCs. Values of bar plots are shown as mean ± s.d.; * p<0.05; *** p<0.001. Data in **C** were analyzed using Mann-Whitney U test.

Phenotyping of *Zc3hc1*$^{-/-}$ mice: The murine homolog of the human *ZC3HC1* gene is ubiquitously expressed in a variety of tissues (**Supplementary Fig 3A-B**). X-Gal staining confirmed that transgenic mice harbored the *LacZ* gene (**Supplementary Fig 3C**) with similar results observed at the DNA level using agarose gel electrophorese for *LoxP* sites (**Figure 4A**). Phenotypically, the birth rate was lower for *Zc3hc1*$^{-/-}$ than for WT and heterozygous animals. To quantify the birth rate, the genotype frequencies were calculated for all genotyped offspring from the mating of *Zc3hc1*-Het mice. The genotype frequencies for *Zc3hc1*$^{-/-}$, WT and Het mice were 10%, 29%, and 61%, respectively. In addition, knockout of *Zc3hc1* had a significant impact on body weight (Figure 4B, left), with lifetime body weight being

significantly lower for *Zc3hc1*$^{-/-}$ than for WT (23±2g vs. 27±5 g; p<0.0001 at 44 weeks) (**Supplementary Figure 3D**). In addition, a few *Zc3hc1*$^{-/-}$ mice exhibited shorter snouts than their WT littermates (**Figure 4 B**, right). Despite the effect of *Zc3hc1* knockout on body weight, life span was similar in *Zc3hc1*$^{-/-}$ and WT mice (**Figure 4B**, bottom).

NIPA deficiency leads to increase neointima formation as a response to injury in mice: Because of the effects of *ZC3HC1* on the *in vitro* migration and proliferation of human SMCs, the role of *Zc3hc1* on neointima formation was assessed *in vivo* using vascular injury model. Neointima formation was induced in *Zc3hc1*$^{-/-}$ and WT mice by wire injury of the femoral artery, and the extent of neointima formation was assessed after 14 days. Neointima formation was approximately 2-fold greater in KO than in WT mice (p=0.005), accompanied by an increase in intima-to-media ratio (p=0.003) (**Figure 4C**). The number of Ki-67 positive cells in the neointima was also significantly greater in KO than in WT mice (21±14 vs. 2±2; p=0.016), with a trend towards more ACTA2 positive cells in KO mice (p=0.087) (**Supplementary Figure 3E-F**). These findings indicate that vascular remodeling after injury is, in part, driven by the proliferation of vascular SMCs.

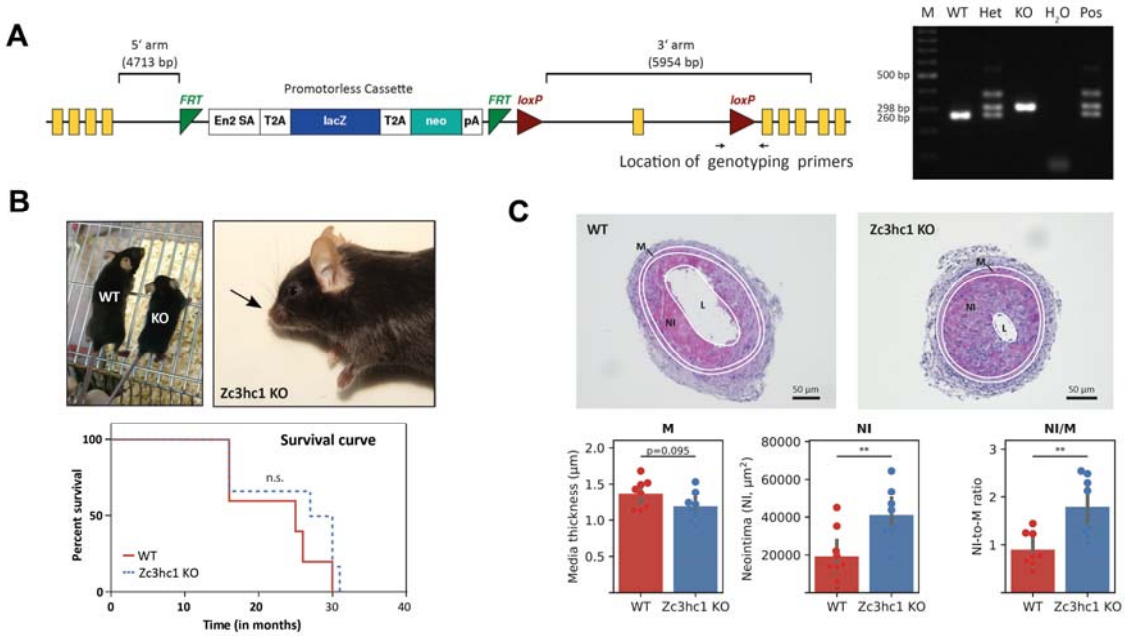

Figure 4. Generation and characteristics of *Zc3hc1*-/- (KO) mice. A) Targeting vector used to generate *Zc3hc1*$^{-/-}$ mice (left) and genotyping of mice by PCR (right) (M: 100 bp marker, Wild-type mice (WT or *Zc3hc1*$^{+/+}$); Het: Heterozygous mice (*Zc3hc1*$^{+/-}$); *Zc3hc1* knockout mice (KO or *Zc3hc1*$^{-/-}$); H_2O; Pos: Positive control represented by Het mice (*Zc3hc1*$^{+/-}$). Location of genotyping primers. Primer pair targeting the intron between exons 5 and 6 of *Zc3hc1*, which contains a *loxP* site (left panel) in the targeted allele. The sizes of the PCR products were 298 bp in KO (*Zc3hc1*$^{-/-}$) and 260 bp in WT (*Zc3hc1*$^{+/+}$) mice, with Het mice (*Zc3hc1*$^{+/-}$) possessing both alleles. **B)** Decreased body weight (left) and abnormally short snout (indicated by arrow) (right) in KO mice. Survival curve showing no statistically significant difference between KO (n=6) and WT (n=5) mice. **C)** Representative hematoxylin & eosin stained femoral artery sections (top), and quantification of media thickness (M), area of neointima formation (NI) and neointima-to-media ratios (NI/M) (bottom) in WT (n=8)

and KO (n=8) mice. Scale bars, 50 µm. Values of the bar plots are shown as mean ± s.d.; ** p<0.01; n.s., not significant. Data were analyzed using Mann-Whitney U test.

Complete lack of NIPA in mouse SMCs increases migration and proliferation: Based on the findings from human SMCs, we isolated primary aortic mouse SMCs and tested whether NIPA deficiency in murine primary aortic SMCs promotes migration and proliferation. Compared with WT SMCs, the migration of *Zc3hc1*$^{-/-}$ SMCs was significantly enhanced at 12 h (p=0.04), but not at later time points (**Figure 5A**). Furthermore, the proliferation of *Zc3hc1*$^{-/-}$ SMCs was significantly greater than that of WT SMCs after 24 h (**Figure 5B**), and the sizes of the nuclei significantly smaller in *Zc3hc1*$^{-/-}$ than in WT SMC (**Figure 5 B**, bottom). These findings suggest that the lack of NIPA promotes SMC migration during the first few hours, with proliferation occurring later.

Knockout of *Zc3hc1* leads to cyclin B1 accumulation in mouse SMC: Because NIPA has been shown to interact with cyclin B1 [13], we compared the expression of Cyclin B1 protein in NIPA-deficient and WT murine SMCs. Western blot analysis confirmed that NIPA-deficient mice lacked *Zc3hc1*encoding protein NIPA (**Figure 5C**, top) leading to a significantly greater accumulation of cyclin B1 in *Zc3hc1*$^{-/-}$ than in WT SMCs (p=0.006) (**Figure 5C**, bottom).

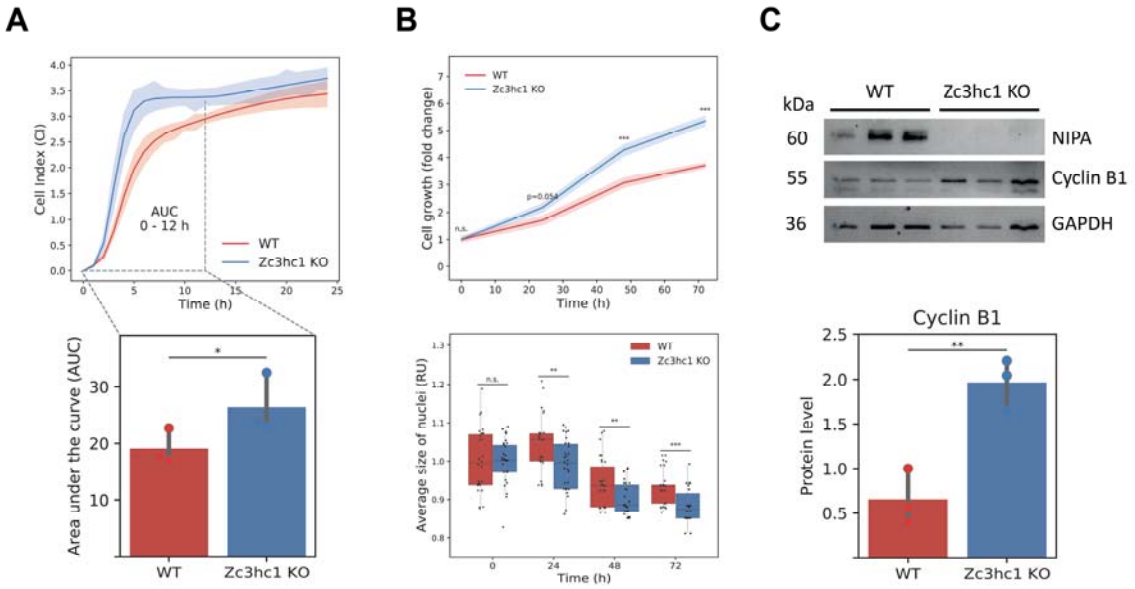

Figure 5. Knockout (KO) of *Zc3hc1* in murine aortic SMCs. SMCs isolated from *Zc3hc1*$^{-/-}$ mice show elevated migration (**A**) and proliferation (**B**) compared with SMCs isolated from wild-type (WT) mice. **C**) Western blotting of NIPA confirming the knockout of *Zc3hc1* in SMCs, resulting in accumulation of cyclin B1 protein. Values of bar plots are shown as mean ± s.d.; * p<0.05; ** p<0.01; *** p<0.001. Data were analyzed using unpaired Student's t test (**B**) or using Mann-Whitney U test (**A** and **C**).

Discussion:

Restenosis is one of the main clinical complications in patients who undergo coronary artery revascularization [32,33]. SMCs not only regulate the arterial contractile tonus and blood pressure but also constitute the key cell type during atherosclerotic plaque formation and in response to revascularization procedures [34–36]. SMCs migrate from the media into the intima of the vessels, followed by alterations in their phenotype in response to their new microenvironment [34–36]. This study assessed the role of *ZC3HC1* on the migration, proliferation and neointima formation of SMCs.

The ubiquitously expressed *ZC3HC1* gene encodes the cell cycle protein NIPA, which has been found first to be associated with CAD in several independent GWASs [2–8]. The CAD-associated rs11556924-C/T SNP in *ZC3HC1* is functional, leading to an amino acid change from arginine to histidine (p.Arg363His) [4,7,9]. Analysis of the publicly available GTEx dataset eQTL (V8) showed that the genetic variant rs11556924-T results in reduced *ZC3HC1* gene expression in heart (atrial appendage and left ventricle) and skin samples. Because eQTL effects are often cell type specific, we tested whether an eQTL was present in aortic SMCs from 151 heart transplant donors[16], finding that SMCs from donors carrying the rs11556924-T allele have lower *ZC3HC1* expression and migrate faster than SMCs from donors carrying the rs11556924-C allele. The absence of a significant association between *ZC3HC1* expression and rs11556924 in blood samples[9], monocytes/macrophages[28] and aortic endothelial cells[29] suggests that the regulatory impact of the variant at the *ZC3HC1* locus is specific to SMCs.

SiRNA mediated knockdown (KD) of *ZC3HC1* in a commercially available human SMC line resulted in increased cell migration during the first 12 h compared with controls. In addition, PDGF-induced proliferation of *ZC3HC1*-KD SMCs was greater than that of control SMCs at 72 h, but not at earlier time points (24–48 h). This may explain the lack of a significant correlation between the rs11556924-T allele and cell proliferation in our study at 24 h. The results obtained with *ZC3HC1*-KD SMCs are contrary to findings showing that siRNA mediated knockdown of NIPA impaired HeLa cell proliferation [9]. This discrepancy may be explained by differences in cell types and differences in proliferation assays, in that the earlier study measured metabolic activity (WST-1 reagent) rather than counting cells.

To assess the molecular mechanisms involved in *ZC3HC1* modulation, we performed transcriptome analysis, followed by analyses of gene–protein interaction networks and pathway enrichment *in vitro*. The increased migration and proliferation of *ZC3HC1*-KD SMCs was partly due to the transition of SMCs from a contractile/quiescent phenotype to a

synthetic/proliferative phenotype [34–37]. This was reflected in part by the downregulation of expression of mRNAs encoding canonical SMC contractile marker genes such as *alpha-smooth muscle actin* (*ACTA2*), *calponin* (*CNN1*), *transgelin* (*TAGLN*), and *leiomodin 1* (*LMOD1*) [34–38]. In addition to these changes in SMC contractile marker genes, our pathway analysis revealed that protein ubiquitination and mitotic cell cycle processes were affected by the knockdown of *ZC3HC1*, presumably through *CCNB1/cyclin B1*. The protein cyclin B1 is a key component in the control of cell cycle progression[13] and was found to be a key regulatory hub in our gene interaction network. Downregulation of *ZC3HC1* or its protein NIPA in human primary SMCs led to the accumulation of cyclin B1 protein, in agreement with previous findings [7,13]. For example, the effect of the *ZC3HC1* missense variant p.Arg363His (rs11556924-T) on proliferation and mitotic progression was assessed using a genome-editing approach in the pseudo-diploid colon carcinoma cell line DLD-1[7]. The change in amino acid was found to alter cyclin B1 dynamics, presumably resulting from enhanced NIPA phosphorylation at Ser395 in cells carrying the T allele. Interestingly, phosphorylated NIPA is degraded during late mitosis[39] and phosphorylation of NIPA abrogates the ability of NIPA to form the CSF^{NIPA} complex and to ubiquitinate cyclin B1[13]. The lack of cyclin B1 ubiquitination accelerates its nuclear accumulation, reducing the time required to complete mitosis[7]. Taken together, these findings indicate that the effect of cyclin B1 on the cell cycle in SMCs may be tightly linked to both enhanced NIPA phosphorylation and decreased level of NIPA protein mediated by the missense variant rs11556924-T (**Figure 6**).

The exact regulatory mechanisms by which NIPA/cyclin B1 regulates gene expression and cellular signaling remain unclear, in particular the roles of SMC contractile marker genes and genes/proteins involved in cell adhesion, the extracellular matrix and cytokine mediated signaling. Many genes involved in protein ubiquitination (e.g., *FBX06*, *RNF7*, *RNF213*, and *RNF182*) and proteasome complex formation (e.g., *PSMB8* and *PSMB9*) are upregulated in *ZC3HC1*-KD SMCs, probably to compensate for the deficiency of NIPA. For example, FBX06 is a component of the SCF-type E3 ubiquitin ligase complex [40] and SCF complexes have been found to control cell proliferation through ubiquitin mediated degradation of critical regulators, including cell cycle proteins (e.g., cyclins) or transcription factors (e.g., β-catenin) [41]. Therefore, NIPA deficiency leading to an increased expression of genes involved in protein ubiquitination may trigger an orchestrated gene regulation accompanied by an ubiquitin mediated degradation of specific transcription factors such as serum response factor (SRF). The transcription factor SRF ($\log_2(FC)=-0.41$; $p_{adj}=1.96 \times 10^{-5}$) targets about one

quarter of differentially expressed genes, including *ZC3HC1* itself, *CCNB1*, and all canonical SMC contractile marker genes[42,43]. Among these SRF target genes, *ANLN* (encoding anillin actin binding protein), which is co-expressed with *CCNB1* (STRING score=0.891; see **Figure 3A**, cluster 3), plays a role in regulating actin cytoskeletal dynamics, cell migration, cytokines, and bleb assembly during mitosis [44,45].

As *ZC3HC1*-KD induced transcriptional changes are rather small, with only 60 genes being up- or downregulated ≥2-fold, many of its effects may take place at the protein level, e.g., due to cyclin B1 accumulation. For example, the CDK1-cyclin B1 complex phosphorylates the protein Mcl-1, a regulator of apoptosis, thereby inducing its degradation [46]. Cyclin B1 also interacts with the diaphanous related formin 3 protein, encoded by *DIAPH3*[47] (STRING score=0.959; see **Figure 3A**, cluster 3), which is required for cytokinesis, stress fiber formation, and transcriptional activation of SRF (UniProt/Q9NSV4[48,49]). Similar to Mcl-1, CDK1-cyclin B1 may also phosphorylate the DIAPH3 protein, leading to its degradation. Taken together, these findings suggest that *ZC3HC1/CCNB1* modulation initiates various steps involving protein ubiquitination and degradation of specific factors that normally maintain the contractile phenotype in human SMCs (**Figure 6**).

To determine whether these *in vitro* findings could be extended to an *in vivo* model, we investigated the effects of complete NIPA KO on vascular remodeling in a mouse model. Similar to human SMCs, SMCs from these mice migrated and proliferated more and had increased cyclin B1 levels compared with SMCs derived from their WT littermates. The increased migratory/proliferative activity of murine SMC due to an accumulation of cyclin B1 may explain the greater degree of injury-induced neointima formation in *Zc3hc1*$^{-/-}$ compared to WT mice. This finding is also in agreement with results demonstrating that increased level of cyclin B1 is associated with enhanced neointima formation[50] and that inhibition of this increase protects against neointima formation [51]. Because only female mice were included in our study, we cannot rule out any sex bias. However, we did not see any sex-stratified effects in our human dataset or in datasets from the UK Biobank (**Supplementary Table 2**). Moreover, male human *ZC3HC1*-KD SMCs behaved similarly to female murine *Zc3hc1*$^{-/-}$ SMCs, suggesting that the impact of NIPA modulation is independent of sex.

Finally, it remains elusive why the T allele in *ZC3HC1* lowers the risk of CAD [4,6,9,10], but increases the risk of carotid IMT as demonstrated recently in 502 patients with rheumatoid arthritis [11]. One reason could be the bivalent role of vascular SMCs as their

584 biological function in atherosclerosis have opposite effects depending on the stage of the
585 lesions (early vs. advanced stage). At early stages of the formation of atherosclerotic lesions,
586 migratory and proliferative SMCs are known to play a detrimental role in atherosclerosis [34,52–
587 54]. Therefore, anti-proliferative therapies were previously proposed for atherosclerosis [55,56]. In
588 contrary, the role of SMCs in advanced lesions is thought to be beneficial by stabilizing the
589 plaque, which may result in an asymptomatic progression of atherosclerosis. Interestingly,
590 two working groups observed that SMCs derived from advanced plaques are less
591 proliferative. Consequently they assumed that enhancement and not inhibition of SMC
592 proliferation may be beneficial for plaque stability in advanced lesions [54,56], thereby reducing
593 the risk of major adverse cardiovascular event outcomes such as MI. Moreover, the T allele
594 also lowers the risk for blood pressure (**Figure 1A**) that is a major risk factor CAD [30,31],
595 probably due to its impact on NIPA gene expression/phosphorylation and SMC contractile
596 genes.
597
598 Taken together, our integrative analyses highlighted the functional role of *ZC3HC1* as
599 a neointima formation-associated gene (**Figure 6**). This might offer clues into potentially
600 targetable SMC mediated disease mechanisms. Additional studies are required to determine
601 the exact molecular mechanisms by which *ZC3HC1* affects SMC proliferation, migration and
602 neointima formation, by, for example, using SMC-lineage tracing mouse models and
603 proteomic approaches. Our findings, however, provide strong evidence that lower *ZC3HC*
604 gene expression in presence of the rs11556924-T allele or genetic manipulation in SMCs
605 increased cell migration and, to some extent, enhanced their proliferation at later stages.
606 Consequently, more proliferation of SMCs increases the risk of early lesion progression and
607 neo-intima formation but may have an advantage in advance lesions by stabilizing the plaque.
608

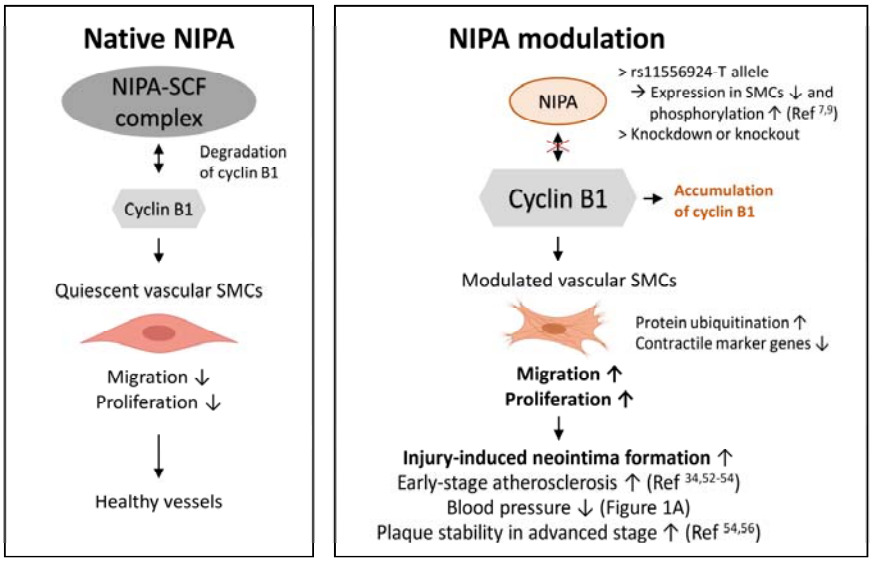

Figure 6: Diagram illustrating the main findings of this study, that a deficiency in *ZC3HC1* increases vascular SMC migration, proliferation, and neointima formation following injury. Under normal (healthy) conditions NIPA, an essential part of the SCF-type E3 ubiquitin ligase complex, activates the degradation of cyclin B1, which reduces SMC migration and proliferation (left). However, *ZC3HC1* modulation (right), by reducing the amount of NIPA or increasing NIPA phosphorylation[7,9], is accompanied by cyclin B1 accumulation and increased SMC migration and proliferation. This in turn leads to injury-induced neointima formation and progression of early-stage atherosclerosis [34,52–54]. On the other hand, the rs11556924-T is associated with lower blood pressure (see **Figure 1A**) and increased SMC proliferation in the late stage of atherosclerosis may contribute to plaque stability [54,56], resulting in an asymptomatic progression of this disease. Cell illustrations are from BioRender.

Author contributions:

Redouane Aherrahrou, Tobias Reinberger, Heribert Schunkert, Thorsten Kessler, Jeanette Erdmann and Zouhair Aherrahrou designed the project. Redouane Aherrahrou, Tobias Reinberger, Jeanette Erdmann and Zouhair Aherrahrou contributed to the text of the main manuscript. Redouane Aherrahrou, Tobias Reinberger, Jaafar Al-Hasani, Julia Werner, Miriam Otto, Sandra Wrobel, Maren Behrensen, and Zouhair Aherrahrou performed the characterization experiments and generated data for most of the figures and tables. Maria Loreto Munoz-Venegas, Mete Civelek and Thorsten Kessler participated in data analysis and lookup. All authors contributed to the final article.

Sources of Funding:

This work was supported by the German Federal Ministry of Education and Research (BMBF) in the context of the German Centre for Cardiovascular Research (FKZ 81Z0700108, FKZ81X2700133); by Fondation Leducq (18CVD02, PlaqOmics); and by the Deutsche Forschungsgemeinschaft (DFG, German Research Foundation) under Germany`s

Excellence Strategy – EXC 22167-390884018 to HB and as part of the collaborative research centers SFB 1123 (B02, to T.K. and H.S.), TRR 267 (B06, to H.S.). This study was also supported by an American Heart Association Postdoctoral Fellowship (18POST33990046, to RA), National Institutes of Health grant (R21 HL135230, to MC), and by the German Federal Ministry of Education and Research (BMBF) in the context of the DZHK-Säule-B projects (FKZ 81X2700121). In addition, this work was supported by the Corona Foundation as part of the Junior Research Group Translational Cardiovascular Genomics (S199/10070/2017).

Acknowledgments:

The authors thank Maren Behrensen, Sandra Wrobel, and Lisa Paurat for technical support. We also thank the members of the Erdmann, Schunkert, and Civelek laboratories for feedback and discussions.

Conflict of interest: The authors declare that there is no conflict of interest.

References:

1. Naghavi M, Abajobir AA, Abbafati C, Abbas KM, Abd-Allah F, Abera SF, Aboyans V, Adetokunboh O, Ärnlöv J, Afshin A, Agrawal A, Kiadaliri AA, Ahmadi A, Ahmed MB, Aichour AN, Aichour I, Aichour MTE, Aiyar S, Al-Eyadhy A, Alahdab F, Al-Aly Z, Alam K, Alam N, Alam T, Alene KA, Ali SD, Alizadeh-Navaei R, Alkaabi JM, Alkerwi A, Alla F, et al. Global, regional, and national age-sex specifc mortality for 264 causes of death, 1980-2016: A systematic analysis for the Global Burden of Disease Study 2016. *The Lancet* 2017;**390**:1151-1210.

2. Samani NJ, Erdmann J, Hall AS, Hengstenberg C, Mangino M, Mayer B, Dixon RJ, Meitinger T, Braund P, Wichmann H-E, Barrett JH, König IR, Stevens SE, Szymczak S, Tregouet D-A, Iles MM, Pahlke F, Pollard H, Lieb W, Cambien F, Fischer M, Ouwehand W, Blankenberg S, Balmforth AJ, Baessler A, Ball SG, Strom TM, Braenne I, Gieger C, Deloukas P, et al. Genomewide association analysis of coronary artery disease. *N Engl J Med* 2007;**357**:443–453.

3. Kathiresan S, Voight BF, Purcell S, Musunuru K, Ardissino D, Mannucci PM, Anand S, Engert JC, Samani NJ, Schunkert H, Erdmann J, Reilly MP, Rader DJ, Morgan T, Spertus JA, Stoll M, Girelli D, McKeown PP, Patterson CC, Siscovick DS, O'Donnell CJ, Elosua R, Peltonen L, Salomaa V, Schwartz SM, Melander O, Altshuler D, Merlini PA, Berzuini C, Bernardinelli L, et al. Genome-wide association of early-onset myocardial infarction with single nucleotide polymorphisms and copy number variants. *Nat Genet* 2009;**41**:334-341.

4. Schunkert H, König IR, Kathiresan S, Reilly MP, Assimes TL, Holm H, Preuss M, Stewart AFR, Barbalic M, Gieger C, Absher D, Aherrahrou Z, Allayee H, Altshuler D, Anand SS, Andersen K, Anderson JL, Ardissino D, Ball SG, Balmforth AJ, Barnes TA, Becker DM, Becker LC, Berger K, Bis JC, Boekholdt SM, Boerwinkle E, Braund PS, Brown MJ, Burnett MS, et al. Large-scale association analysis identifies 13 new susceptibility loci for coronary artery disease. *Nat Genet* 2011;**43**:333-338.

5. Lu X, Wang LL, Chen S, He L, Yang X, Shi Y, Cheng J, Zhang L, Gu CC, Huang J, Wu T, Ma Y, Li J, Cao J, Chen JJJ, Ge D, Fan Z, Li YYY, Zhao L, Li H, Zhou X, Chen L, Liu DD, Chen JJJ, Duan X, Hao

Y, Wang LL, Lu F, Liu Z, Yao C, et al. Genome-wide association study in Han Chinese identifies four new susceptibility loci for coronary artery disease. *Nat Genet* 2012;**44**:890–894.

6. Nikpay M, Goel A, Won H-H, Hall LM, Willenborg C, Kanoni S, Saleheen D, Kyriakou T, Nelson CP, Hopewell JC, Webb TR, Zeng L, Dehghan A, Alver M, Armasu SM, Auro K, Bjonnes A, Chasman DI, Chen S, Ford I, Franceschini N, Gieger C, Grace C, Gustafsson S, Huang J, Hwang S-J, Kim YK, Kleber ME, Lau KW, Lu X, et al. A comprehensive 1000 Genomes–based genome-wide association meta-analysis of coronary artery disease. *Nat Genet* Nature Publishing Group; 2015;**47**:1121–1130.

7. Jones PD, Kaiser MA, Najafabadi MG, McVey DG, Beveridge AJ, Schofield CL, Samani NJ, Webb TR. The Coronary Artery Disease-associated Coding Variant in Zinc Finger C3HC-type Containing 1 (ZC3HC1) Affects Cell Cycle Regulation *. *J Biol Chem* Elsevier; 2016;**291**:16318–16327.

8. Ishigaki K, Akiyama M, Kanai M, Takahashi A, Kawakami E, Sugishita H, Sakaue S, Matoba N, Low S-K, Okada Y, Terao C, Amariuta T, Gazal S, Kochi Y, Horikoshi M, Suzuki K, Ito K, Koyama S, Ozaki K, Niida S, Sakata Y, Sakata Y, Kohno T, Shiraishi K, Momozawa Y, Hirata M, Matsuda K, Ikeda M, Iwata N, Ikegawa S, et al. Large-scale genome-wide association study in a Japanese population identifies novel susceptibility loci across different diseases. *Nat Genet* 2020;**52**:669–679.

9. Linseman T, Soubeyrand S, Martinuk A, Nikpay M, Lau P, McPherson R. Functional Validation of a Common Nonsynonymous Coding Variant in ZC3HC1 Associated With Protection From Coronary Artery Disease. *Circ Cardiovasc Genet* 2017;**10**:e001498.

10. Harst P van der, Verweij N. Identification of 64 Novel Genetic Loci Provides an Expanded View on the Genetic Architecture of Coronary Artery Disease. *Circ Res* 2018;**122**:433–443.

11. López-Mejías R, Genre F, García-Bermúdez M, Corrales A, González-Juanatey C, Llorca J, Miranda-Filloy JA, Rueda-Gotor J, Blanco R, Castañeda S, Martín J, González-Gay MA. The ZC3HC1 rs11556924 polymorphism is associated with increased carotid intima-media thickness in patients with rheumatoid arthritis. *Arthritis Res Ther* 2013;**15**:R152.

12. Ouyang T, Bai R-Y, Bassermann F, Klitzing C von, Klumpen S, Miething C, Morris SW, Peschel C, Duyster J. Identification and Characterization of a Nuclear Interacting Partner of Anaplastic Lymphoma Kinase (NIPA) *. *J Biol Chem* Elsevier; 2003;**278**:30028–30036.

13. Bassermann F, Klitzing C von, Münch S, Bai R-Y, Kawaguchi H, Morris SW, Peschel C, Duyster J. NIPA Defines an SCF-Type Mammalian E3 Ligase that Regulates Mitotic Entry. *Cell* 2005;**122**:45–57.

14. Smolock E, Berk BC. Chapter 98 - Vascular Smooth Muscle Cell Remodeling in Atherosclerosis and Restenosis. In: Hill JA, Olson EN, eds. *Muscle* Boston/Waltham: Academic Press; 2012. p. 1301–1309.

15. Moser J, Ark J van, Dijk MC van, Greiner DL, Shultz LD, Goor H van, Hillebrands J-L. Distinct Differences on Neointima Formation in Immunodeficient and Humanized Mice after Carotid or Femoral Arterial Injury. *Sci Rep* 2016;**6**:35387.

16. Aherrahrou R, Guo L, Nagraj VP, Aguhob A, Hinkle J, Chen L, Yuhl Soh J, Lue D, Alencar GF, Boltjes A, Laan SW van der, Farber E, Fuller D, Anane-Wae R, Akingbesote N, Manichaikul AW, Ma L, Kaikkonen MU, Björkegren JLM, Önengüt-Gümüşcü S, Pasterkamp G, Miller CL, Owens GK, Finn A, Navab M, Fogelman AM, Berliner JA, Civelek M. Genetic Regulation of Atherosclerosis-Relevant Phenotypes in Human Vascular Smooth Muscle Cells. *Circ Res* 2020;**127**:1552–1565.

17. Dobin A, Davis CA, Schlesinger F, Drenkow J, Zaleski C, Jha S, Batut P, Chaisson M, Gingeras TR. STAR: ultrafast universal RNA-seq aligner. *Bioinforma Oxf Engl* 2013;**29**:15–21.

18. DeLuca DS, Levin JZ, Sivachenko A, Fennell T, Nazaire M-D, Williams C, Reich M, Winckler W, Getz G. RNA-SeQC: RNA-seq metrics for quality control and process optimization. *Bioinforma Oxf Engl* 2012;**28**:1530–1532.

19. Liang Y, Aguet F, Barbeira AN, Ardlie K, Im HK. A scalable unified framework of total and allele-specific counts for cis-QTL, fine-mapping, and prediction. *Nat Commun* 2021;**12**:1424.

20. Song G, Lin D, Bao L, Jiang Q, Zhang Y, Zheng H, Gao Q. Effects of High Glucose on the Expression of LAMA1 and Biological Behavior of Choroid Retinal Endothelial Cells. *J Diabetes Res* 2018;**2018**:7504614.

21. Livak KJ, Schmittgen TD. Analysis of relative gene expression data using real-time quantitative PCR and the 2(-Delta Delta C(T)) Method. *Methods San Diego Calif* 2001;**25**:402–408.

22. Aherrahrou Z, Doehring LC, Ehlers E-M, Liptau H, Depping R, Linsel-Nitschke P, Kaczmarek PM, Erdmann J, Schunkert H. An alternative splice variant in Abcc6, the gene causing dystrophic calcification, leads to protein deficiency in C3H/He mice. *J Biol Chem* 2008;**283**:7608–7615.

23. Love MI, Huber W, Anders S. Moderated estimation of fold change and dispersion for RNA-seq data with DESeq2. *Genome Biol* 2014;**15**:550.

24. Franceschini A, Szklarczyk D, Frankild S, Kuhn M, Simonovic M, Roth A, Lin J, Minguez P, Bork P, Mering C von, Jensen LJ. STRING v9.1: protein-protein interaction networks, with increased coverage and integration. *Nucleic Acids Res* 2013;**41**:D808–D815.

25. Kessler T, Zhang L, Liu Z, Yin X, Huang Y, Wang Y, Fu Y, Mayr M, Ge Q, Xu Q, Zhu Y, Wang X, Schmidt K, Wit C de, Erdmann J, Schunkert H, Aherrahrou Z, Kong W. ADAMTS-7 inhibits re-endothelialization of injured arteries and promotes vascular remodeling through cleavage of thrombospondin-1. *Circulation* 2015;**131**:1191–1201.

26. Hemani G, Zheng J, Elsworth B, Wade KH, Haberland V, Baird D, Laurin C, Burgess S, Bowden J, Langdon R, Tan VY, Yarmolinsky J, Shihab HA, Timpson NJ, Evans DM, Relton C, Martin RM, Davey Smith G, Gaunt TR, Haycock PC. The MR-Base platform supports systematic causal inference across the human phenome. *eLife* 2018;**7**:e34408.

27. Buniello A, MacArthur JAL, Cerezo M, Harris LW, Hayhurst J, Malangone C, McMahon A, Morales J, Mountjoy E, Sollis E, Suveges D, Vrousgou O, Whetzel PL, Amode R, Guillen JA, Riat HS, Trevanion SJ, Hall P, Junkins H, Flicek P, Burdett T, Hindorff LA, Cunningham F, Parkinson H. The NHGRI-EBI GWAS Catalog of published genome-wide association studies, targeted arrays and summary statistics 2019. *Nucleic Acids Res* 2019;**47**:D1005–D1012.

28. Rotival M, Zeller T, Wild PS, Maouche S, Szymczak S, Schillert A, Castagné R, Deiseroth A, Proust C, Brocheton J, Godefroy T, Perret C, Germain M, Eleftheriadis M, Sinning CR, Schnabel RB, Lubos E, Lackner KJ, Rossmann H, Münzel T, Rendon A, Consortium C, Erdmann J, Deloukas P, Hengstenberg C, Diemert P, Montalescot G, Ouwehand WH, Samani NJ, Schunkert H, et al. Integrating Genome-Wide Genetic Variations and Monocyte Expression Data Reveals Trans-Regulated Gene Modules in Humans. Barsh GS, ed. *PLoS Genet* 2011;**7**:e1002367.

29. Erbilgin A, Civelek M, Romanoski CE, Pan C, Hagopian R, Berliner JA, Lusis AJ. Identification of CAD candidate genes in GWAS loci and their expression in vascular cells. *J Lipid Res* 2013;**54**:1894–1905.

30. Hajar R. Risk Factors for Coronary Artery Disease: Historical Perspectives. *Heart Views Off J Gulf Heart Assoc* 2017;**18**:109–114.

31. Khera AV, Kathiresan S. Genetics of coronary artery disease: Discovery, biology and clinical translation. 2017;**18**:331-344.

32. Welt FGP, Rogers C. Inflammation and Restenosis in the Stent Era. *Arterioscler Thromb Vasc Biol* American Heart Association; 2002;**22**:1769–1776.

33. Kim MS, Dean LS. In-Stent Restenosis. *Cardiovasc Ther* 2011;**29**:190–198.

34. Grootaert MOJ, Bennett MR. Vascular smooth muscle cells in atherosclerosis: time for a re-assessment. *Cardiovasc Res* 2021;**0**:1–14.

35. Sorokin V, Vickneson K, Kofidis T, Woo CC, Lin XY, Foo R, Shanahan CM. Role of Vascular Smooth Muscle Cell Plasticity and Interactions in Vessel Wall Inflammation. *Front Immunol* Frontiers; 2020;**11**.

36. Goikuria H, Freijo M del M, Manrique RV, Sastre M, Elizagaray E, Lorenzo A, Vandenbroeck K, Alloza I. Characterization of Carotid Smooth Muscle Cells during Phenotypic Transition. *Cells* 2018;**7**.

37. Rensen SSM, Doevendans PAFM, Eys GJJM van. Regulation and characteristics of vascular smooth muscle cell phenotypic diversity. *Neth Heart J* 2007;**15**:100–108.

38. Alsaigh T, Evans D, Frankel D, Torkamani A. Decoding the transcriptome of atherosclerotic plaque at single-cell resolution. *bioRxiv* Cold Spring Harbor Laboratory; 2020;2020.03.03.968123.

39. Klitzing C von, Huss R, Illert AL, Fröschl A, Wötzel S, Peschel C, Bassermann F, Duyster J. APC/C(Cdh1)-mediated degradation of the F-box protein NIPA is regulated by its association with Skp1. *PloS One* 2011;**6**:e28998.

40. Zhang Y-W, Brognard J, Coughlin C, You Z, Dolled-Filhart M, Aslanian A, Manning G, Abraham RT, Hunter T. The F box protein Fbx6 regulates Chk1 stability and cellular sensitivity to replication stress. *Mol Cell* 2009;**35**:442–453.

41. Willems AR, Schwab M, Tyers M. A hitchhiker's guide to the cullin ubiquitin ligases: SCF and its kin. *Biochim Biophys Acta* 2004;**1695**:133–170.

42. Miano JM, Long X, Fujiwara K. Serum response factor: master regulator of the actin cytoskeleton and contractile apparatus. *Am J Physiol Cell Physiol* 2007;**292**:C70-81.

43. Rouillard AD, Gundersen GW, Fernandez NF, Wang Z, Monteiro CD, McDermott MG, Ma'ayan A. The harmonizome: a collection of processed datasets gathered to serve and mine knowledge about genes and proteins. *Database* 2016;**2016**.

44. Zhao W-M, Fang G. Anillin is a substrate of anaphase-promoting complex/cyclosome (APC/C) that controls spatial contractility of myosin during late cytokinesis. *J Biol Chem* 2005;**280**:33516–33524.

45. Straight AF, Field CM, Mitchison TJ. Anillin binds nonmuscle myosin II and regulates the contractile ring. *Mol Biol Cell* 2005;**16**:193–201.

46. Phosphorylation of Mcl-1 by CDK1–cyclin B1 initiates its Cdc20-dependent destruction during mitotic arrest. *EMBO J* John Wiley & Sons, Ltd; 2010;**29**:2407–2420.

47. Wan C, Borgeson B, Phanse S, Tu F, Drew K, Clark G, Xiong X, Kagan O, Kwan J, Bezginov A, Chessman K, Pal S, Cromar G, Papoulas O, Ni Z, Boutz DR, Stoilova S, Havugimana PC, Guo X, Malty RH, Sarov M, Greenblatt J, Babu M, Derry WB, Tillier ER, Wallingford JB, Parkinson J, Marcotte EM, Emili A. Panorama of ancient metazoan macromolecular complexes. *Nature* 2015;**525**:339–344.

48. Tominaga T, Sahai E, Chardin P, McCormick F, Courtneidge SA, Alberts AS. Diaphanous-related formins bridge Rho GTPase and Src tyrosine kinase signaling. *Mol Cell* 2000;**5**:13–25.

49. Baarlink C, Wang H, Grosse R. Nuclear actin network assembly by formins regulates the SRF coactivator MAL. *Science* 2013;**340**:864–867.

50. Braun-Dullaeus RC, Mann MJ, Seay U, Zhang L, Der Leyen HE von, Morris RE, Dzau VJ. Cell cycle protein expression in vascular smooth muscle cells in vitro and in vivo is regulated through phosphatidylinositol 3-kinase and mammalian target of rapamycin. *Arterioscler Thromb Vasc Biol* 2001;**21**:1152–1158.

51. Morishita R, Gibbons GH, Kaneda Y, Ogihara T, Dzau VJ. Pharmacokinetics of antisense oligodeoxyribonucleotides (cyclin B1 and CDC 2 kinase) in the vessel wall in vivo: enhanced therapeutic utility for restenosis by HVJ-liposome delivery. *Gene* 1994;**149**:13–19.

52. Sandison ME, Dempster J, McCarron JG. The transition of smooth muscle cells from a contractile to a migratory, phagocytic phenotype: direct demonstration of phenotypic modulation. *J Physiol* 2016;5**94**:6189–6209.

811 53. Allahverdian S, Chaabane C, Boukais K, Francis GA, Bochaton-Piallat M-L. Smooth muscle cell fate and
812 plasticity in atherosclerosis. *Cardiovasc Res* 2018;**114**:540–550.

813 54. Bennett MR, Sinha S, Owens GK. Vascular Smooth Muscle Cells in Atherosclerosis. *Circ Res* American
814 Heart Association; 2016;**118**:692–702.

815 55. Andrés V, Castro C. Antiproliferative strategies for the treatment of vascular proliferative disease. *Curr*
816 *Vasc Pharmacol* 2003;**1**:85–98.

817 56. O'Brien ER, Alpers CE, Stewart DK, Ferguson M, Tran N, Gordon D, Benditt EP, Hinohara T, Simpson
818 JB, Schwartz SM. Proliferation in primary and restenotic coronary atherectomy tissue. Implications for
819 antiproliferative therapy. *Circ Res* American Heart Association; 1993;**73**:223–231.

820